Direct simulations of cavity tones by the finite difference lattice Boltzmann method

Tsutahara, Michihisa

Tajiri, Shinsuke

Direct simulations of cavity tones by the finite difference lattice Boltzmann method

Shinsuke Tajiri, Michihisa Tsutahara*
Graduate School of Engineering
Kobe University, 1-1 Rokko, Nada, Kobe 657-8501 Japan
*tutahara@mech.kobe-u.ac.jp

1 INTRODUCTION

The cavity tones are important aerodynamic phenomena relating the aerodynamic noise of high-speed vehicles. The sound generation mechanism is known to include a feedback mechanism. Theoretically, this phenomena are usually analyzed in base of the incompressible flows for low Mach number flows [1][2]. In this case, the most important factor is the stability of the shear layer separated from the trailing edge of the cavity. The stability of the shear layer is known to be affected by the sound generated at the leading edge. But the detail is not clear.

The mechanism will be clarified by the direct simulation that calculates the shear layer and the generated sound simultaneously. The lattice Boltzmann method [3]-[7] has been known to simulate such flows easily. In this paper, we present compressible model for the finite difference lattice Boltzmann method (FDLBM) [8]. The authors have been applying the FDLBM to aero-acoustic problems, such as the Aeolian tones and the edge tones, and obtained sufficient results [9][10].

In this paper, we apply this model to simulate two-dimensional cavity tones, and perform the direct simulation of this phenomenon..

2 FINITE DIFFERENCE LATTICE BOLTZMANN METHOD

2.1 Two-dimensional Lattice Boltzmann model for compressible flows

. The equation to be solved is the following discretized Bhatnager- Gross-Krook (BGK) equation [10]

$$\frac{\partial f_i(t,\mathbf{r})}{\partial t} + c_{i\alpha}\frac{\partial f_i(t,\mathbf{r})}{\partial r_\alpha} - \frac{Ac_{i\alpha}}{\tau}\frac{\partial(f_i - f_i^{(0)})}{\partial r_\alpha} = -\frac{1}{\tau}\left[f_i(t,\mathbf{r}) - f_i^{(0)}(t,\mathbf{r})\right] \qquad (1)$$

where f_i is the particle distribution function at time t and position **r,** subscripts i represents the direction of particle translation and α the Cartesian coordinates, $f_i^{(0)}$ on the RHS is the local equilibrium distribution function, $\mathbf{c}_i$ is the particle velocity, and

τ is called the single relaxation time factor. The third term on LHS represents the negative viscosity term when the constant A is positive.

The macroscopic variables for continuous fluids are given from f_i taking the moments of $\mathbf{c}_i$ as:

Density $\rho = \sum_i f_i$ (2)

Momentum $\rho u_\alpha = \sum_i f_i c_{i\alpha}$ (3)

Energy $\frac{1}{2}\rho u^2 + \rho e = \sum_i \frac{1}{2} f_i c_i^2$ (4)

where e is the internal energy per unit mass. The constraints that determine the form of the local equilibrium distribution function are

Density $\rho = \sum_i f_i^{(0)}$ (5)

Momentum $\rho u_\alpha = \sum_i f_i^{(0)} c_{i\alpha}$ (6)

Energy $\frac{1}{2}\rho u^2 + \rho e = \sum_i \frac{1}{2} f_i^{(0)} c_i^2$ (7)

Momentum flux $p\delta_{\alpha\beta} + \rho u_\alpha u_\beta = \sum_i f_i^{(0)} c_{i\alpha} c_{i\beta}$ (8)

Energy flux $\left(\frac{1}{2}\rho u^2 + \rho e\right) u_\alpha = \sum_i \frac{1}{2} f_i^{(0)} c_i^2 c_{i\alpha}$ (9)

. Definition of the variables in the same forms by particle distribution function in (2) to (4), and its local equilibrium state in (5) to (7) means that to the above variables, mass, momentum and energy of the fluid particle, are conserved in the collision stage.

The local equilibrium distribution function can be defined as

$$f_a^{(0)} = F_a \rho[1 - 2B(\mathbf{c}_a \cdot \mathbf{u}) + 2B^2(\mathbf{c}_a \cdot \mathbf{u})^2 + B(\mathbf{u} \cdot \mathbf{u}) - \frac{4}{3}B^3(\mathbf{c}_a \cdot \mathbf{u})^3 - 2B^2(\mathbf{c}_a \cdot \mathbf{u})(\mathbf{u} \cdot \mathbf{u})] \quad (10)$$

where subscript a represents the kind of particles and their moving directions, and will be written as $a = p, k, i$, and p and k are given in Table 1, respectively. The constants are determined for two-dimensional flows as follows [7].

$$F_0 = 1 + \frac{5}{4Bc^2}\left(\frac{17}{96B^2c^4} + \frac{35}{48Bc^2} + \frac{49}{45}\right) \quad (11a)$$

$$F_{11} = -\frac{1}{8Bc^2}\left(\frac{13}{16B^2c^4} + \frac{71}{24Bc^2} + 3\right) \quad (11b)$$

$$F_{12} = \frac{1}{16Bc^2}\left(\frac{5}{16B^2c^4} + \frac{25}{24Bc^2} + \frac{3}{5}\right) \quad (11c)$$

$$F_{13} = -\frac{1}{24Bc^2}\left(\frac{1}{16B^2c^4} + \frac{1}{8Bc^2} + \frac{1}{15}\right) \quad (11d)$$

$$F_{21} = \frac{1}{4B^3c^6}\left(\frac{Bc^2}{3} + \frac{1}{8}\right) \tag{11e}$$

$$F_{22} = -\frac{1}{1536B^3c^6}\left(2Bc^2 + 3\right) \tag{11f}$$

$$B = -\frac{1}{2e} \tag{11g}$$

2.2 Navier-Stokes equations

The Chapman-Enscog expansion is applied to the lattice BGK equation (1), and we obtain the following Navier-Stokes equations for compressible fulids

$$\frac{\partial \rho}{\partial t} + \frac{\partial}{\partial r_\alpha}\left(\rho u_\alpha\right) = 0 \tag{12}$$

$$\frac{\partial}{\partial t}(\rho u_\alpha) + \frac{\partial}{\partial r_\beta}\left(\rho u_\alpha u_\beta\right) = -\frac{\partial P}{\partial r_\alpha} + \frac{\partial}{\partial r_\beta}\mu\left(\frac{\partial u_\beta}{\partial r_\alpha} + \frac{\partial u_\alpha}{\partial r_\beta}\right) + \frac{\partial}{\partial r_\alpha}\left(\lambda\frac{\partial u_\gamma}{\partial r_\gamma}\right) \tag{13}$$

$$\begin{aligned}&\frac{\partial}{\partial t}\left(\rho e + \frac{1}{2}\rho u^2\right) + \frac{\partial}{\partial r_\alpha}\left(\rho e + P + \frac{1}{2}\rho u^2\right)u_\alpha \\ &\quad = \frac{\partial}{\partial r_\alpha}\left(\kappa'\frac{\partial e}{\partial r_\alpha}\right) + \frac{\partial}{\partial r_\alpha}\left\{\mu u_\beta\left(\frac{\partial u_\beta}{\partial r_\alpha} + \frac{\partial u_\alpha}{\partial r_\beta}\right)\right\} + \frac{\partial}{\partial r_\alpha}\left(\lambda\frac{\partial u_\beta}{\partial r_\beta}u_\alpha\right)\end{aligned} \tag{14}$$

where, the pressure p, the viscosity μ, the second viscosity λ, and the thermal conductivity κ'are

$$p = \rho e, \quad \mu = \frac{2}{D}\rho e\tau(\phi - A),$$

$$\lambda = -\frac{4}{D^2}\rho e\tau(\phi - A) = -\frac{2}{D}\mu, \kappa' = \frac{2(D+2)}{D^2}\tau\rho e(\phi - A) \tag{15a,b,c,d}$$

and the speed of sound c_s is given as

$$c_s = \sqrt{\frac{2(D+2)}{D^2}e} \tag{16}$$

In (15) and (16), D is the dimension, and in this study $D = 2$.

2.3 Turbulent model

The basic principle in a LES is that large scale motions are resolved and only unresolved small scale motions are modeled. To realize this, one needs a scale separation decomposing the unknowns into a local average $\overline{f}$ (large scale) and a subgrid-scale component f'(small scale), where $f = \overline{f} + f'$ stands for instantaneous value of a quantity, by applying the filtering operation:

$$\overline{f}(t,x)=\int_{-\infty}^{\infty} G(t,y)\, f(x-y)\,dy \tag{17}$$

To transform the governing equation into one depending only on local averages, the filter operator is applied to the discrete BGK equation:

$$\frac{\partial \overline{f}_i}{\partial t}+c_{i\alpha}\frac{\partial \overline{f}_i}{\partial x_\alpha}-Ac_{i\alpha}\frac{\partial}{\partial x_\alpha}\frac{\overline{f_i-f_i^{(0)}}}{\phi_{total}}=-\frac{1}{\phi_{total}}\left(\overline{f}_i-\overline{f}_i^{(0)}\right) \tag{18}$$

where the relaxation parameter ϕ_{total} is variable depending on time and space. ϕ_{total} shows the effects of the subgrid-scale component, and a constant A is the same as the one in (1).

2.3.1 Dynamic Smagorinsky model

We use the dynamic Smagorinsky model (DSM) proposed by Germano [11]. The DSM is sub-grid scale eddy viscosity model for incompressible flows, but this works are carried out in low Mach number flows using this model.

Smagorinsky proposed the first subgrid –scale stress model. In this model, the anisotropic part of the subgrid-scale stress tensor takes the Boussinesq eddy viscosity form:

$$\tau_{\alpha\beta}-\frac{\delta_{\alpha\beta}}{3}\tau_{\gamma\gamma}=-2\nu_t\overline{S}_{\alpha\beta} \tag{19}$$

$$\tau_{\alpha\beta}=\overline{u_\alpha u_\beta}-\overline{u}_\alpha\overline{u}_\beta \tag{20}$$

$$\overline{S}_{\alpha\beta}=\frac{1}{2}\left(\frac{\partial u_\alpha}{\partial x_\beta}+\frac{\partial u_\beta}{\partial x_\alpha}\right) \tag{21}$$

where $\overline{S}_{\alpha\beta}$ is the strain tensor of filtered velocity, ν_t is the subgrid eddy-viscosity coefficient and $\delta_{\alpha\beta}$ is the Kronecker delta. Subgrid eddy-viscosity ν_t is

$$\nu_t=C\Delta^2\left|\overline{S}\right| \quad \text{with} \quad \left|\overline{S}\right|=\sqrt{2\overline{S}_{\alpha\beta}\overline{S}_{\alpha\beta}} \tag{22}$$

Here, C is the square of the Smagorinsky constant C_s. Δ is the filter width (grid size) and is taken to be the geometric average of the grid spacing in three directions, $\Delta=\left(\Delta x\Delta y\Delta z\right)^{1/3}$.

The major defect of the Smagorinsky model is the choice of constant C_s as there is no standard way of choosing this constant. Ad hoc adjustments have to be made for different flow type and non-equilibrium flows to account properly for energy dissipation. With the desire to eliminate these problems, the dynamic model was proposed by Germano et al. In this model, along with Lilly's modification [12], and C is determined by

$$C=-\frac{\lambda_{mn}M_{mn}}{M_{kl}M_{kl}} \tag{23}$$

where the tensors on RHS of (23) are expressed as

$$\lambda_{\alpha\beta}=\widetilde{\overline{u}_\alpha\overline{u}_\beta}-\tilde{\overline{u}}_\alpha\tilde{\overline{u}}_\beta \tag{24}$$

$$M_{\alpha\beta} = \tilde{\bar{\Delta}}^2 \left|\tilde{\bar{S}}\right| \tilde{\bar{S}}_{\alpha\beta} - \widetilde{\bar{\Delta}^2 \left|\tilde{\bar{S}}\right| \tilde{\bar{S}}_{\alpha\beta}} \tag{25}$$

2.3.2 Subgrid Model for FDLBM

When we employ subgrid model for FDLBM, we determine ϕ_{total} as follows in D2Q21 model:

$$\nu_{total} = \frac{2}{3} e\left(\phi_{total} - A\right) \quad \text{with} \quad \nu_{total} = \nu + \nu_t \tag{26}$$

2.4 Finite difference schene

For the space discretization we use the fourth order central finite difference scheme added by the numerical viscosity term.

$$c_x \frac{\partial f_i}{\partial x} = c_x \frac{f_{i-2} - 8 f_{i-1} + 8_{i+1} - f_{i+2}}{12\Delta x} + \alpha \frac{|c_x|}{12} \frac{f_{i-2} - 4 f_{i-1} + 6 f_i - 4 f_{i+1} + f_{i+2}}{\Delta x} \tag{27}$$

where $\alpha = 1$ corresponds to the third-order upwind scheme UTOPIA.

The time integration we employ the second order Runge-Kutta method as

$$f_i^{n+\frac{1}{2}} = f_i^n + \frac{1}{2}\Delta t \left[-c_{i\alpha} \frac{\partial f_i^n}{\partial x_\alpha} + \frac{A}{\phi} c_{i\alpha} \frac{\partial\left(f_i^n - f_i^{(0)\,n}\right)}{\partial x_\alpha} - \frac{1}{\phi}\left(f_i^n - f_i^{(0)\,n}\right) \right]$$

$$f_i^{n+1} = f_i^n + \Delta t \left[-c_{i\alpha} \frac{\partial f_i^{n+\frac{1}{2}}}{\partial x_\alpha} + \frac{A}{\phi} c_{i\alpha} \frac{\partial\left(f_i^{n+\frac{1}{2}} - f_i^{(0)\,n+\frac{1}{2}}\right)}{\partial x_\alpha} - \frac{1}{\phi}\left(f_i^{n+\frac{1}{2}} - f_i^{(0)\,n+\frac{1}{2}}\right) \right] \tag{28}$$

3 TWO-DIMENSIONAL CAVITY TONES

We perform the direct simulations of the cavity tones using above mentioned Finite difference lattice Boltzmann model.

The computational domain is shown in Fig.1 in which the square cavity with the width 0.02m and the depth 0.02m is located in the flat plate of the length 2.02m. The flow region is taken 1.16m above the plate. The boundary condition for outer boundary is fixed as the uniform flow with velocity 68m/s. The gas density ρ is 1.206 kg/m^3, and the kinematic viscosity ν is assumed very small value of 3×10^{-8} m^2/s for the sake of easiness of the sound generation . Then the Mach number of the uniform flow is 0.2, and the Reynolds number based on the cavity width is 5.47×10^7.

The grid system is shown in Fig.2. The number of grid is 361×283 and the non-uniform grid system is employed.

The pressure is estimated by the following non-dimensional value

$$p^* = \frac{p - p_0}{p_0} \qquad (29)$$

where p_0 represents the uniform flow pressure. The asterisk is omitted hereafter.

3.1 Laminar flow simulation

3.1.1 Dipole-like mode

First we perform a simulation for laminar flows. The initial condition is the uniform flow everywhere. So there appears a strong compression wave (like shock wave) in the cavity and it moves inside the cavity. This reciprocal motion of the wave emits the dipole-like sound as shown in Fig.3 at time of 0.02 sec, where the red part is positive pressure region and the blue part represents the negative pressure region. The compression waves decays soon by the viscosity.

3.1.2 Monopole-like emission mode

After this dipole-like mode, there appears a monopole-like emission at time 0.168sec as shown in Fig.4, in which whole the pressure inside the cavity changes cyclically positive and negative. The flow pattern at the same time shows that the shear layer separated from the trailing edge of the cavity vibrates up and down, but the amplitude is not large. This mode continue considerably long. So this mode is considered to be the main mode for the cavity tone phenomenon in this case. The wave-length of the sound is about 0.23m.

Even in this mode, the sound pressure field is not symmetrical with respect to the flow direction as shown in Fig.5, in which the horizontal distribution in (b) is that along the line 0.01m above the plate and in (b) that along the line perpendicular to the flow direction is shown. Red and blue lines represent the lines proportional to $x^{-0.5}$ to which the sound pressure distribution obey. Sound propagation is not isotropic.

Figure 5(a) shows that the pattern is simple on the windward side, but it is rather complicated on the lee side. The pressure distribution along the line perpendicular to the flow is also complicated. These facts indicate that the sound emission is not exactly a monopole-mode. However, in the far field the pattern becomes simpler and the sound field looks like monopole emission.

This characteristic is true for the above mentioned dipole-like emission. Probably, even in this mode, the vibration of the air inside the cavity may play an important part of the sound emission.

The history of the sound pressure at a point on the line perpendicular to the flow and the horizontal velocity fluctuation of the shear layer is shown in Fig.6. In the shear

layer, three points are taken, one of which is located at the center between the two edges of the cavity and other two are taken at points about 2mm above and below the point. The horizontal velocity becomes slower on the lower side of the shear layer, but the amplitude of the fluctuation is larger. The frequencies in the three points are the same. The frequencies of the sound and the shear layer fluctuation are different, and the sound wave frequency is about 1500 Hz and that of the shear layer fluctuation is about 1350 Hz. The difference of the period between the two about 10%, and the vibration of the shear layer is slower.

3.1.3 Sound emission mode in which the vortex inside the cavity moves out to the flow

Finally, we detect another mode, in which the structure of the vortexes inside the cavity changes and the vortex near the trailing edge moves out to the flow periodically as shown in Fig.7. In this case, the sound emission is basically monotonic, but the sound pressure field is seen to be complex, especially in the near field. This mode continue too, and the feed-back mechanism should be exist.

3.1.4 The feed-back mechanism

The feed-back mechanism is examined for the last mode. The pressure, the vortexes, and the velocity vectors inside the cavity over the one period are shown in Fig.8. The first row shows the situation when the pressure inside the cavity rises and the positive pressure sound is just emitted. The gas inside the cavity expands. Then the pressure inside the cavity drops, and the shear layer declines downward as shown in the third row. At the same time, the stream-line opens at the trailing edge and some fluid flows out. Even so, the pressure inside the cavity rises again as shown in the last row. The feed-back mechanism will be performed through the whole region inside the cavity because the pressure inside the cavity changes as a whole. It is also understood that the small pressure change causes the large change of the flow pattern.

3.2 Turbulent flow simulation

The simulation using above mentioned turbulent model for the two-dimensional cavity tone. For turbulent simulation, it is seen that the sound is detected slightly more easily than laminar simulation, but the difference is not clear. It is well known that the resonance occurs more wide frequencies for the turbulent flow. Of course, finer structure of the vortexes are not resolved by the same grid as for the laminar case. But in three-dimensional calculations, we have obtained the difference in spectra in turbulent flow and laminar flow [13]. Finer grids will be needed or, probably, for three-dimensional simulations, the difference may take place.

4 CONCLUSIONS

Direct simulation of the cavity tone is performed by the finite difference lattice Boltzmann method. It is shown that there are several modes of the sound emission, and that the near field of the sound pressure is not isotropic. The relationship between the sound emission and the flow inside the cavity is visually shown and the feed-back mechanism is clarified.

REFERENCES

[1] M.S. Howe, Edge, cavity and aperture tones at very low Mach numbers, J. Fluid Mech., 330, 61-84, 1997

[2]. M.S. Howe, Acoustics of Fluid-Structure Interactions, Cambridge University Press,1998.

[3] D.A. Wolf-Gladrow, Lattice-gas cellular automata and lattice Boltzmann models, Lecture Notes in Mathematics, Springer 2000

[4] Y.H. Qian, S. Succi, S.A. Orszag, Recent advances in lattice Boltzmann computing, Ann. Rev. of Comp. Phy. III, D. Stauffer ed. World Scientific, 19951

[5] S Chen, G.D. Doolen, Lattice Boltzmann method for fluid flows, Ann. Rev. Fluid Mech.30, Ann. Rev. Inc. 1998.

[6] S. Succi, The lattice Boltzmann equation for fluid dynamics and beyond, Oxford, 2001.

[7] M. Tsutahara, N. Takada, T. Kataoka, Lattice gas and lattice Boltzmann methods, Corona-sha, 1999; in Japanese.

[8] N.S. Cao, S. Chen, S. Jin, D. Martinez, Physical symmetry and lattice symmetry in the lattice Boltzmann method, Phys. Rev., E, 55: R21-R24, 1997.

[9] M. Tsutahara, M. Kurita and T. Kataoka, Direct simulation of Aeolian tone by the finite difference Lattice Boltzmann method, Computational Fluid Dynamics 2002, 508-513, 2003.

[10] M. Tsutahara, T. Kataoka and K. Shikata, Direct simulations of aerodynamic sound by the finite difference Lattice Boltzmann Method, Computational Mechanics, WCCM VI in conjunction with APCOM'04, Beijing, China, Sept.5-10, 1-1, 2004.

[11] M. Germano et al., A dynamic subgrid-scale eddy viscosity model, *Phys. Fluids*, A 3-7, 1760-1765, 1991.

[12] D..K. Lilly, A proposed modification of the Germano subgrid-scale closure model, *Phys. Fluids*, A 4-4, 633-635, 1992.

[13] M. Hiraishi and M. Tsutahara, Direct Simulation of Aerodynamic Sound by the Finite Difference Lattice Boltzmann Method Employing Sub-Grid Model of Turbulence,

Table 1 Velocity set for D3Q21 model

p	k	$\mathbf{c}_{pki} = \left(c_{pkix}, c_{pkiy}\right)$	$c_{pk} = \left\|\mathbf{c}_{pki}\right\|$
0	0	(0,0)	0
1	1	(1,0),(0,1),(-1,0),(0,-1)	1
1	2	(2,0),(0,2),(-2,0),(0,-2)	2
1	3	(3,0),(0,3),(-3,0),(0,-3)	3
2	1	(1,1),(-1,1),(-1,-1),(1,-1)	$\sqrt{2}$
2	2	(2,2),(-2,2),(-2,-2),(2,-2)	$2\sqrt{2}$

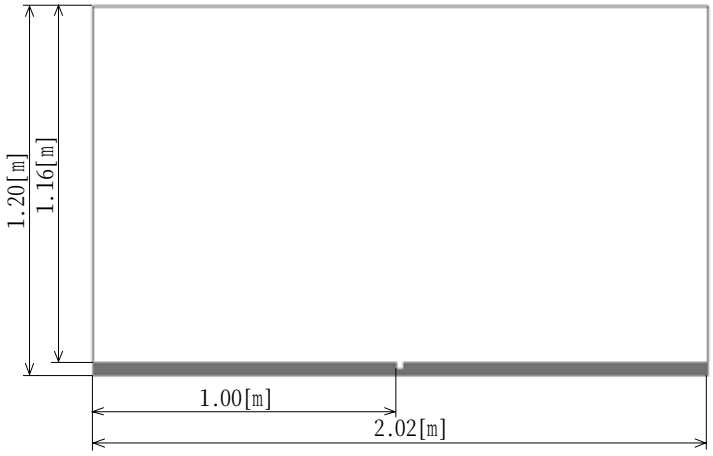

Fig.1 Computational domain

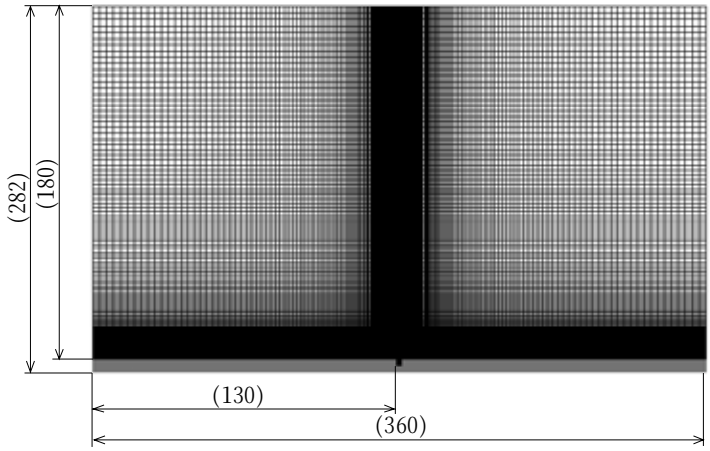

Fig.2 Grid system

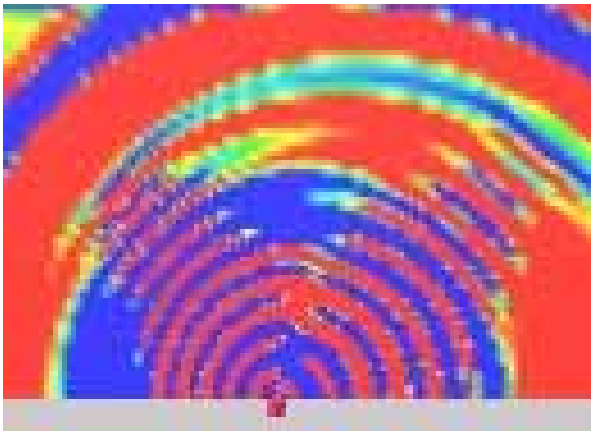

Fig.3 The dipole-like sound emission in early stage

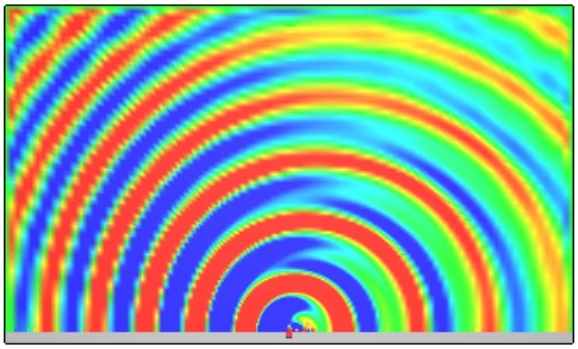

(a) Sound pressure field

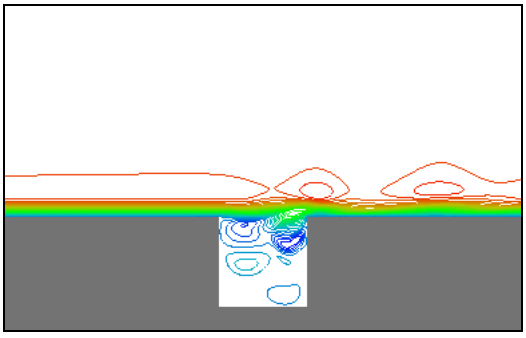

(b) Stream-lines around the cavity

Fig.4 The monopole-like sound emission

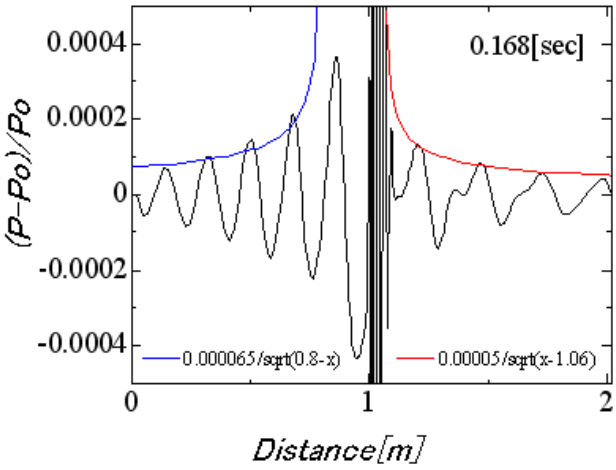

(a) Sound pressure distribution along the flow direction

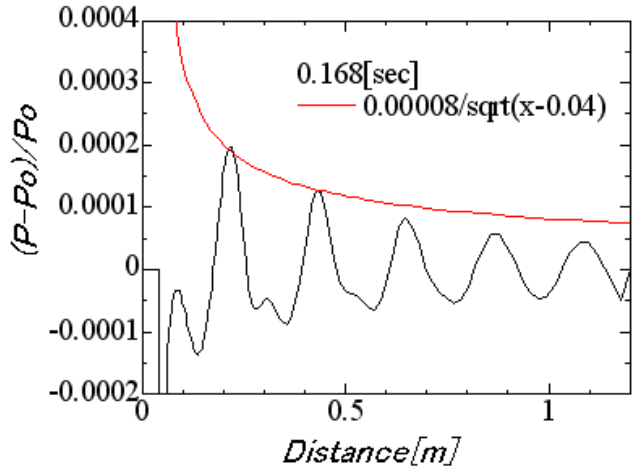

(b) Sound pressure distribution along the perpendicular direction to the flow

Fig.5 Sound pressure distribution

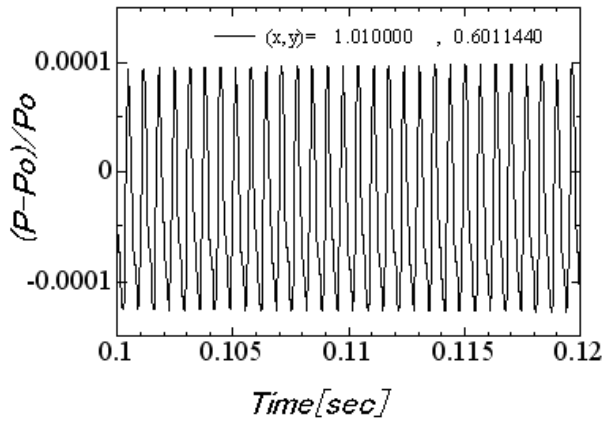

(a) Sound pressure history

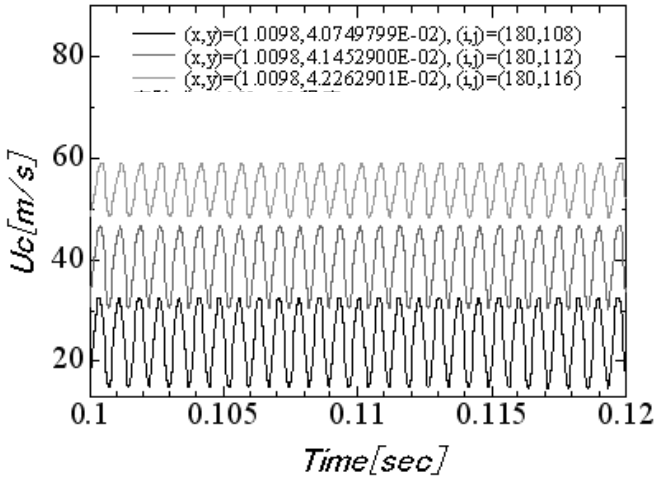

(b) Horizontal velocities and their fluctuations in the shear layer

Fig.6 Relationship between sound pressure and shear layer fluctuation

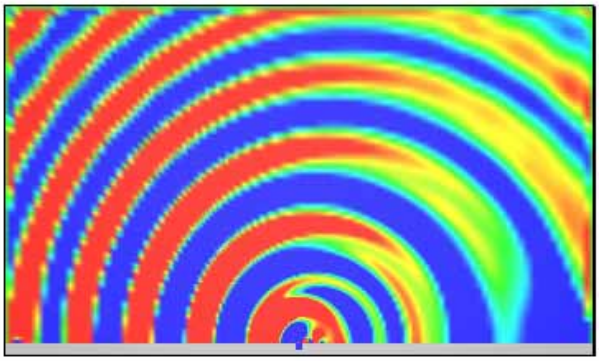

Fig.7 Sound emission mode in which the vortex inside the cavity moves out to the flow

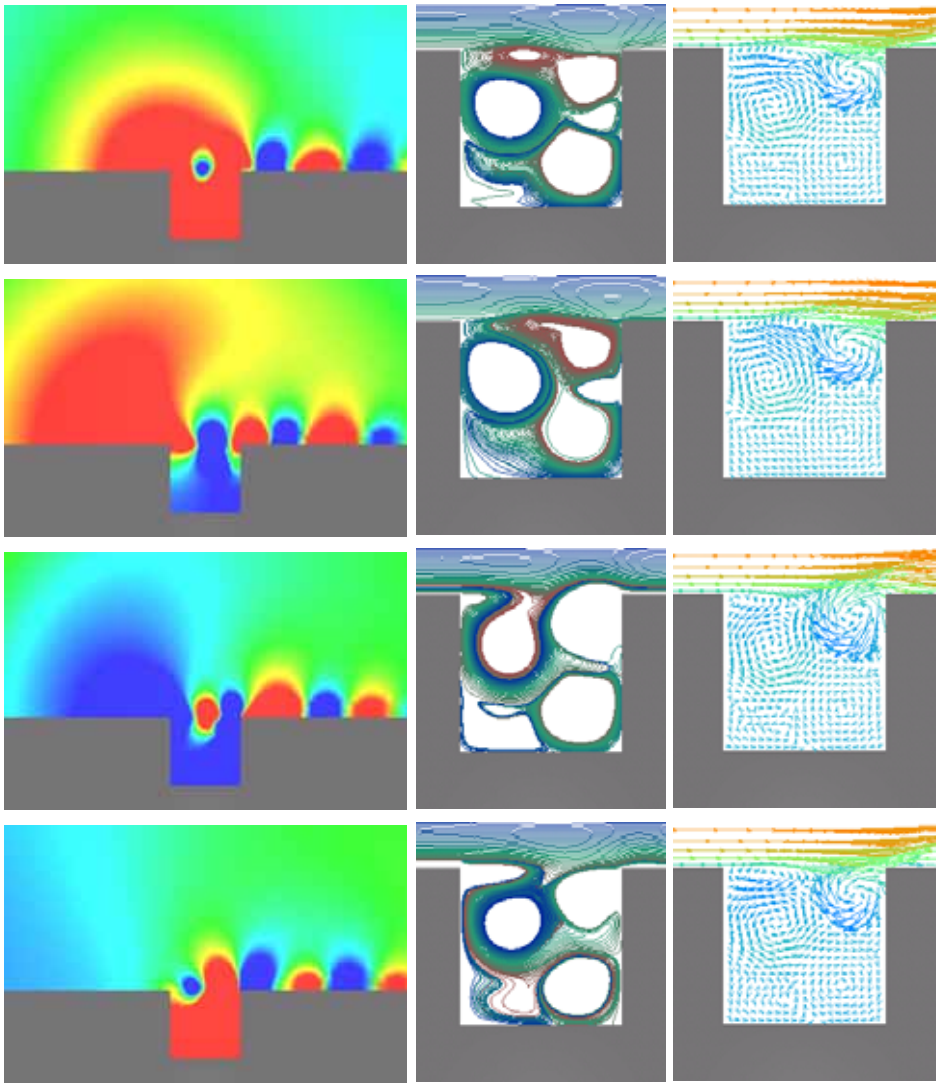

Fig.8 Pressure, vorticity and flow velocity in the cavity